Strong dependence of ultracold chemical rates on electric dipole moments

Goulven Quéméner and John L. Bohn
JILA, University of Colorado, Boulder, Colorado 80309-0440, USA
(Received 25 November 2009; published 4 February 2010)

We use the quantum threshold laws combined with a classical capture model to provide an analytical estimate of the chemical quenching cross sections and rate coefficients of two colliding particles at ultralow temperatures. We apply this quantum threshold model (QT model) to indistinguishable fermionic polar molecules in an electric field. At ultracold temperatures and in weak electric fields, the cross sections and rate coefficients depend only weakly on the electric dipole moment d induced by the electric field. In stronger electric fields, the quenching processes scale as $d^{4(L+\frac{1}{2})}$ where $L > 0$ is the orbital angular-momentum quantum number between the two colliding particles. For p-wave collisions ($L = 1$) of indistinguishable fermionic polar molecules at ultracold temperatures, the quenching rate thus scales as d^6. We also apply this model to pure two-dimensional collisions and find that chemical rates vanish as d^{-4} for ultracold indistinguishable fermions. This model provides a quick and intuitive way to estimate chemical rate coefficients of reactions occuring with high probability.

DOI: 10.1103/PhysRevA.81.022702 PACS number(s): 34.50.Cx, 34.50.Lf

I. INTRODUCTION

Ultracold samples of bialkali polar molecules have been created very recently in their ground electronic $^1\Sigma$, vibrational $v = 0$, and rotational $N = 0$ states [1–3]. This is a promising step before achieving Bose-Einstein condensates or degenerate Fermi gases of polar molecules, provided that further evaporative cooling is efficient. For this purpose, elastic collision rates must be much faster than inelastic quenching rates. This issue is somewhat problematic for the bialkali molecules recently created, since they are subject to quenching via chemical reactions. If a reaction should occur, the products are no longer trapped.

For alkali metal dimers that possess electric dipole moments, elastic scattering appears to be quite favorable, since elastic-scattering rates are expected to scale with the fourth power of the dipole moment [4,5]. Inelastic collisions of polar species can originate from two distinct sources. The long-range dipole-dipole interaction itself is anisotropic and can cause dipole orientations to be lost. This kind of loss generally leads to high inelastic rates and is regarded as the reason why electrostatic trapping of polar molecules is likely not feasible [6]. Moreover, these collisions also scale as the fourth power of dipole moment in the ultracold limit [4], meaning that the ratio of elastic to inelastic rates does not in general improve at higher electric fields. This sort of loss can be prevented by trapping the molecules in optical dipole traps.

More serious is the possibility that collisions are quenched by chemical reactions. Chemical reaction rates are known to be potentially quite high even at ultracold temperatures [7–17]. Indeed, for collision energies above the Bethe-Wigner threshold regime, it appears that many quenching rates, chemical or otherwise, of barrierless systems are well described by applying Langevin's classical model [18]. In this model the molecules must surmount a centrifugal barrier to pass close enough to react but are assumed to react with unit probability when they do so. This model has adequately described several cold molecule quantum dynamics calculations [10,11,13,16,17].

Within the Bethe-Wigner limit, scattering can be described by an elegant quantum defect theory (QDT) approach [19–22]. This approach makes explicit the dominant role of long-range forces in controlling how likely the molecules are to approach close to one another. Consequently, quenching rate constants can often be written in an analytic form that contains a small number of parameters that characterize short-range physics such as chemical reaction probability. For processes in which the quenching probability is close to unity, the QDT theory provides remarkably accurate quenching rates [23,24]. For dipoles, however, the full QDT theory remains to be formulated.

In this article we combine two powerful ideas—suppression of collisions due to long-range physics and high-probability quenching inelastic collisions for those that are not suppressed—to derive simple estimates for inelastic- and reactive-scattering rates for ultracold fermionic dipoles. The theory arrives at remarkably simple expressions of collision rates, without the need for the full machinery of close-coupling calculations. Strikingly, the model shows that quenching collisions scale as the *sixth* power of the dipole moment for ultracold p-wave collisions. On the one hand, this implies a tremendous degree of control over chemical reactions by simply varying an electric field, complementing alternative proposals for electric field control of molecule-molecule [25] or atom-molecule [26] chemistry. On the other hand, it also implies that evaporative cooling of polar molecules may become more difficult as the field is increased. In Sec. II, we formulate the theoretical model for three dimensional collisions. In Sec. III, we apply this model to pure two dimensional collisions and conclude in Sec. IV. In the following, quantities are expressed in S.I. units, unless explicitly stated otherwise. Atomic units (a.u.) are obtained by setting $\hbar = 4\pi\varepsilon_0 = 1$.

II. COLLISIONS IN THREE DIMENSIONS

A. Cross sections and collision rates

In quantum mechanics, the quenching cross section of a pair of colliding molecules (or any particles) of reduced mass

μ for a given collision energy E_c and a partial wave L, M_L is given by

$$\sigma^{qu}_{L,M_L} = \frac{\hbar^2\pi}{2\mu E_c} \left|T^{qu}_{L,M_L}\right|^2 \Delta, \tag{1}$$

where T^{qu} is the transition matrix element of the quenching process, $|T^{qu}_{L,M_L}|^2$ represents the quenching probability, and the factor Δ represents symmetrization requirements for identical particles [27]. If the two colliding molecules are in different internal quantum states (distinguishable molecules), $\Delta = 1$ and if the two colliding molecules are in the same internal quantum state (indistinguishable molecules), $\Delta = 2$. The total quenching cross section of a pair of molecules is $\sigma^{qu} = \sum_{L,M_L} \sigma^{qu}_{L,M_L}$. The quenching rate coefficient of a pair of molecules for a given temperature T (collisional event rate) is given by

$$K^{qu}_{L,M_L} = \langle \sigma^{qu}_{L,M_L}\, v \rangle = \int_0^\infty \sigma^{qu}_{L,M_L} v f(v)\, dv, \tag{2}$$

where

$$f(v) = 4\pi \left(\frac{\mu}{2\pi k_B T}\right)^{3/2} v^2 \exp\left[-(\mu v^2)/(2k_B T)\right] \tag{3}$$

is the Maxwell–Boltzmann distribution for the relative velocities for a given temperature and k_B is the Maxwell-Boltzmann constant. The total quenching rate coefficient of a pair of molecules is $K^{qu} = \sum_{L,M_L} K^{qu}_{L,M_L}$. To avoid confusion, we will also write the corresponding rate equation for collisions between distinguishable and indistinguishable molecules. First, we consider collisions between two distinguishable molecules in quantum states a and b [$\Delta = 1$ in Eq. (1)]. During a time $dt = \tau$, where τ is the time of a quenching collisional event, the number of molecules N_a lost in each collision is one and the number of molecules N_b lost in each collision is one. Then $dN_a/dt = -1/\tau$ and $dN_b/dt = -1/\tau$. The volume per colliding pairs of molecules is $V/(N_a N_b)$, where V stands for the volume of the gas. During the time τ, the quenching collisional event is associated with a volume $\langle \sigma^{qu} v \rangle \tau = K^{qu}\tau$. By definition of τ, this volume should be equal to the one occupied by just one colliding pair of molecules. Then we get $K^{qu}\tau = V/(N_a N_b)$. The rate equation for the number of molecule N_a or N_b is then given by

$$\frac{dN_{a,b}}{dt} = -K^{qu}\frac{N_a N_b}{V}. \tag{4}$$

If $n_a = N_a/V$ and $n_b = N_b/V$ are the densities of molecule a and b in the gas, then

$$\frac{dn_{a,b}}{dt} = -K^{qu} n_a n_b. \tag{5}$$

We consider now the case of collisions between two indistinguishable molecules [$\Delta = 2$ in Eq. (1)]. During the time $dt = \tau$ the number of molecules N lost in each collision is two. Then we get $dN/dt = -2/\tau$. The volume per colliding pairs of molecules is $V/[N(N-1)/2]$ where we have taken into account the indistinguishability of the molecules. For the same reason explained above, the volume associated with the collisional event during the time τ should be equal to the volume occupied by just one colliding pair of molecules. And then $K^{qu}\tau = V/[N(N-1)/2]$. The rate equation for the number of molecule N is then given by

$$\frac{dN}{dt} = -2K^{qu}\frac{N(N-1)/2}{V}. \tag{6}$$

If $n = N/V$ and $N(N-1) \approx N^2$, then

$$\frac{dn}{dt} = -K^{qu} n^2. \tag{7}$$

B. Quantum threshold model

We consider the case of two identical ultracold fermionic, polar molecules, as has been achieved very recently for KRb dimers [2,28] in their ro-vibronic ($^1\Sigma$, $v = 0$, $N = 0$) ground state. Under these circumstances, because of Fermi exchange symmetry, the relative orbital angular-momentum quantum number L between the two molecules must take odd values $L = 1, 3, 5, 7....$ These molecules are polar molecules and can be controlled by an electric field $\mathcal{E}$. In the usual basis set of partial waves $|LM_L\rangle$, the long-range behavior of two colliding polar molecules in a presence of an electric field is governed by an interaction potential matrix whose elements are

$$\langle LM_L|V(R)|L'M'_L\rangle = \left\{\frac{\hbar^2 L(L+1)}{2\mu R^2} - \frac{C_6}{R^6}\right\}\delta_{L,L'}\delta_{M_L,M'_L} - \frac{C_3(L,L';M_L)}{R^3}\delta_{M_L,M'_L}, \tag{8}$$

where R denotes the distance between the two molecules. The diagonal elements represent effective potentials for the colliding molecules and the nondiagonal elements represent couplings between them. The coefficient C_6 is the van der Waals coefficient, assumed to be isotropic in the present treatment. The $-C_3/R^3$ is the term corresponding to the electric dipole-dipole interaction expressed in the partial-wave basis set $\langle LM_L|V_{dd}(R,\theta,\varphi)|L'M'_L\rangle$ between two polarized molecules in the electric field direction, with $V_{dd}(R,\theta,\varphi) = d^2(1-3\cos^2\theta)/(4\pi\varepsilon_0 R^3)$, where $d = d(\mathcal{E})$ is the induced electric dipole moment and θ, φ represent the relative orientation between the molecules. In the basis set of partial waves, C_3 takes the form

$$C_3(L,L';M_L) = \alpha(L,L';M_L)\frac{d^2}{4\pi\varepsilon_0} = 2(-1)^{M_L}\sqrt{2L+1}\sqrt{2L'+1}\begin{pmatrix} L & 2 & L' \\ 0 & 0 & 0\end{pmatrix} \times \begin{pmatrix} L & 2 & L' \\ -M_L & 0 & M'_L\end{pmatrix}\frac{d^2}{4\pi\varepsilon_0}. \tag{9}$$

The large bracket symbols denote the usual $3-j$ coefficients. The coefficient α is introduced to simplify further notations. The combination between repulsive and attractive terms in the effective potentials (diagonal terms) of Eq. (8) generate a potential barrier of height V_b which is plotted schematically in Fig. 1. The height of this barrier plays a crucial role as it can prevent the molecule from accessing the short-range region where reactive chemistry occurs.

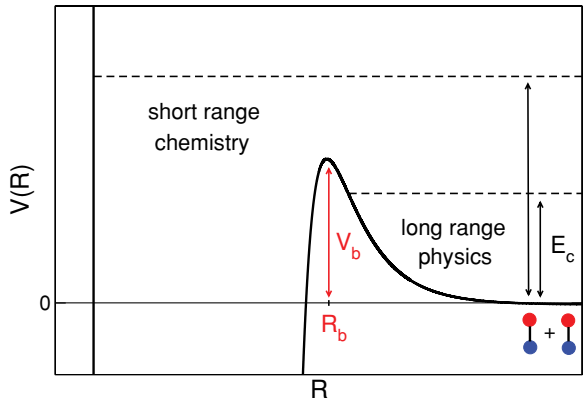

FIG. 1. (Color online) Effective potential barrier $V(R)$ as a function of the intermolecular separation R. V_b and R_b denote the height and the position of the centrifugal barrier.

The quantum threshold (QT) model consists of two conditions. First, for $E_c < V_b$, we use the Bethe-Wigner threshold laws [29,30] for ultracold scattering. Second, we use the classical capture model (Langevin model) [18] to estimate the probability of quenching for $E_c \geqslant V_b$. A classical capture model is indiferent to collision energies $E_c < V_b$ since the barrier prevents the molecules from coming close together. In real-life quantum scattering, collisions do occur at these energies due to quantum tunneling, and they are the ones relevant to ultracold collisions. Moreover, collisions in this energy regime are dictated by the the Bethe-Wigner quantum threshold laws. For quenching collisions, the threshold laws [29–31] state that $|T^{qu}_{L,M_L}|^2 \propto E_c^{L+\frac{1}{2}}$. For $E_c \geqslant V_b$, a classical capture model will guarantee to deliver the molecule pair to small values of R, where chemical reactions are likely to occur with unit probability (see Fig. 1). Following this classical argument, we will assume that when $E_c \geqslant V_b$, the quenching probability reaches unitarity $|T^{qu}|^2 = 1$. Using this assumption together with the quantum threshold laws, the QT quenching tunneling probability below the barrier can be written as

$$\left|T^{qu}_{L,M_L}\right|^2 = \left(\frac{E_c}{V_b}\right)^{L+1/2}. \tag{10}$$

Consequently, the quenching cross section and rate coefficient are approximated by

$$\begin{aligned} \sigma^{qu}_{L,M_L} &= \frac{\hbar^2\pi}{2\mu V_b^{L+\frac{1}{2}}} E_c^{L-\frac{1}{2}}\Delta \\ K^{qu}_{L,M_L} &= \frac{\hbar^2\pi}{\sqrt{2\mu^3}V_b^{L+\frac{1}{2}}} \langle E_c^L\rangle\Delta \end{aligned} \tag{11}$$

for $E_c < V_b$. The QT model has the simple and intuitive advantage of showing how the cross sections and rate coefficients scale with the height of the entrance centrifugal barrier. For $E_c \geqslant V_b$, it is easy to find the corresponding expression of the cross section in Eq. (1) by setting $|T^{qu}|^2 = 1$. The cross section σ^{qu}_{L,M_L} will reach the unitarity limit at $E_c \geqslant V_b$. It is also easy to find the corresponding expression of the rate coefficient in Eq. (2). The QT model is general for any collision between two particles provided that there is a barrier in the entrance collision channel and that chemical reactions occur with near unit probability at short range. The only information on short-range chemistry is that chemical reactions occur at full and unit probability and the only information on long-range physics is provided by the height of the entrance barrier V_b. The QT model describes the background-scattering process, it does not take into account scattering resonances. Note that the model will not be appropriate in the present form for barrierless (s wave) collisions since $V_b = 0$. For this particular type of collisions that do not possess a centrifugal barrier, the QDT theory can be usefully applied [22,32,33]. The present form of the QT model does not take into account the anisotropy of the intermolecular potential at intermediate range and/or the electronic and nuclear spin structure of the molecular complex but remains suitable as far as the entrance centrifugal barrier takes place at long range. The QT model will have to be modified if longer range interactions take place. For example, collisions between $N = 0$ and $N = 1$ polar molecules can have long-range interactions between hyperfine states due to dipolar and hyperfine couplings [27,34]. However, for collisions between rotationless $N = 0$ polar molecules, the hyperfine couplings are weak and the QT model can be applied without further modifications.

C. Rates in zero electric field

In the absence of an electric field in Eq. (8), the long-range potential reduces to a diagonal term in the basis set of partial waves. The position and height of the barrier are given by

$$\begin{aligned} R_b &= \left[\frac{6\mu C_6}{\hbar^2 L(L+1)}\right]^{1/4} \\ V_b &= \left\{\frac{[\hbar^2 L(L+1)]^3}{54\mu^3 C_6}\right\}^{1/2}. \end{aligned} \tag{12}$$

We can insert Eq. (12) in Eq. (11) to get analytical forms of the quenching cross section or rate coefficient. For two indistinguishable fermionic polar molecules at ultracold temperatures when $L = 1$, we get

$$K^{qu}_{L=1,M_L} = \frac{\pi}{8}\left(\frac{3^{13}\mu^3 C_6^3}{\hbar^{10}}\right)^{1/4} k_B T\Delta. \tag{13}$$

In Eq. (11), we used the fact that $\langle E_c\rangle = 3k_BT/2$ in three dimensions. Note that to get the overall contribution for a given L, we have to multiply Eq. (13) by the degeneracy factor $(2L+1)$ corresponding to all values of M_L. We can get similar expressions for any partial wave L.

To test the validity of the model, we compare in Fig. 2 the quenching cross sections of $^{39}\mathrm{K}(^2S) + ^{39}\mathrm{K}_2(^3\Sigma_u^+, v = 1, N = 0)$ collisions as a function of the collision energy for the partial waves $L = 1 - 5$: (i) calculated in Ref. [10] with a full quantum time-independent close-coupling calculation based on hyperspherical democratic coordinates [35] and the full potential energy surface of K_3 (solid lines) and (ii) using the simple QT model (dashed lines) with a value of $C_6 = 9050$ a.u. given in Ref. [10] (1 a.u. = 1 $E_h a_0^6$, where E_h is the Hartree energy and a_0 is the Bohr radius). In this example, the QT model provides an upper limit to the cross sections. This is due to the fact that the quenching cross section does not reach a maximum value at the height of the barrier V_b, but

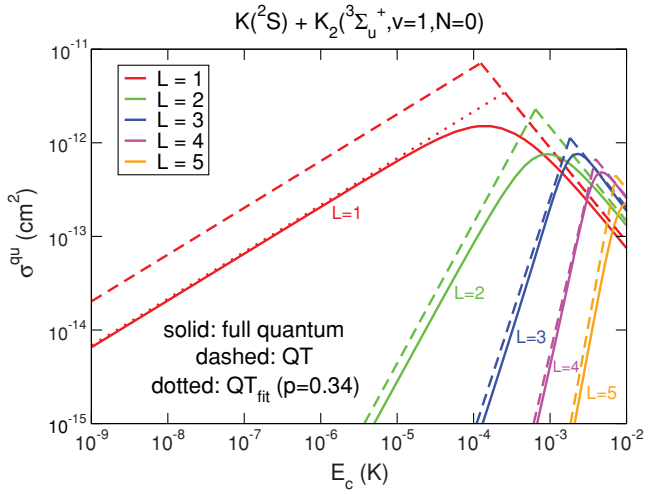

FIG. 2. (Color online) Quenching cross section of $^{39}\mathrm{K} + {}^{39}\mathrm{K}_2$ as a function of the collision energy for the partial wave $L = 1 - 5$: (i) calculated with a full quantum calculation (solid lines), reproduced from Ref. [10], (ii) using the QT model (dashed lines), (iii) fitting the QT model (dotted line), using $p = 0.34$ in Eq. (14).

rather at somewhat higher energy, say $\gamma \times V_b$, with $\gamma > 1$ (see Ref. [10]). For all partial waves, there is a worse agreement for collision energies in the vicinity of the height of the barrier where the passage from the ultralow regime to the unitarity limit is smoother than for the QT model. This smoother passage is visible in Fig. 3 for the full quantum $L = 1$ quenching probability compared to the QT model, which has a sharp corner in the vicinity of V_b.

To account for more flexibility in the QT model, one can replace V_b in Eq. (10) by $\gamma \times V_b$ ($\gamma > 1$) and use the coefficient γ as a fitting parameter to reproduce either full quantum calculations or experimental observed data. Alternatively, we can correct the QT quenching tunneling probability with an

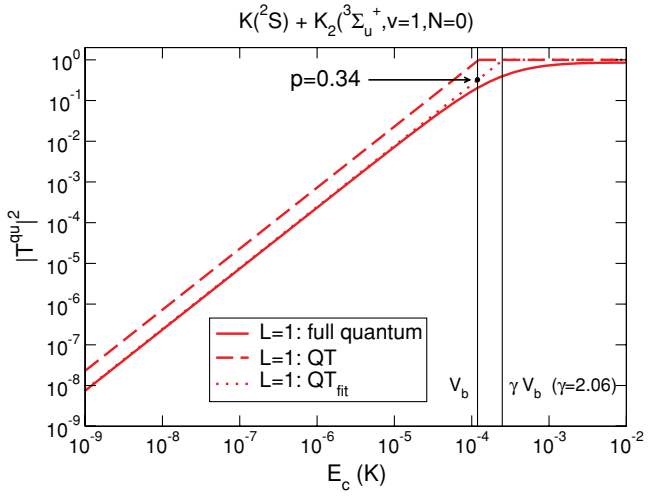

FIG. 3. (Color online) Quenching probability of $^{39}\mathrm{K} + {}^{39}\mathrm{K}_2$ as a function of the collision energy for the partial wave $L = 1$: comparison between the full quantum calculation (solid line) and the QT model (dashed line). The fitted QT model appears as a dotted line. The height of the barrier V_b and the corrected height $\gamma \times V_b (\gamma = 2.06)$ appear as vertical lines.

overall factor p,

$$\left|T^{qu}_{L,M_L}\right|^2_{\mathrm{fit}} = p \times \left(\frac{E_c}{V_b}\right)^{L+1/2} \tag{14}$$

with $p = \gamma^{-(L+1/2)}$. $p < 1$ can be interpreted as the quenching probability reached at the height of the barrier V_b in the QT model rather than the rough full unit probability ($p = 1$). As an example, we find that $\gamma \approx 2.06$ reproduces the quantum $L = 1$ partial-wave cross section for $^{39}\mathrm{K} + {}^{39}\mathrm{K}_2$ (dotted line in Fig. 2 and Fig. 3). This yields a maximum quenching probability of $p = \gamma^{-3/2} \approx 0.34$ instead of 1. In other words, the QT model is only a factor of $p^{-1} \approx 2.96$ higher than the full quantum calculation for $^{39}\mathrm{K} + {}^{39}\mathrm{K}_2$ collisions at ultralow energies.

Given the fact that full quantum calculations are computationally demanding [8–14] and impossible at the present time for alkali molecule-molecule collisions, the accuracy of the QT model is satisfactory and can be a quick and powerful alternative way to estimate orders of magnitude for the scattering observables. Besides, agreement between the QT model with experimental data or full quantum calculations is expected to be satisfactory for collisions involving alkali species, because it is likely that short-range quenching couplings will dominate and lead to high quenching probability in the region where the two particles are close together [16]. Very recently, Eq. (13) of the QT model has been applied for the evaluation of ultracold chemical quenching rate of collisions of two $^{40}\mathrm{K}^{87}\mathrm{Rb}$ molecules in the same internal quantum state and provided good agreement with the experimental data [32].

D. Rates in nonzero electric field

1. *Numerical expressions*

In the presence of an electric field in Eq. (8), the long-range interaction potential matrix is no more diagonal and couplings between different values of L occur. M_L is still a good quantum number. A first approximation (diabatic approximation) consists of neglecting these couplings and using only the diagonal elements of the diabatic matrix directly. Then one can find numerically for which R the centrifugal barriers are maximum and evaluate the height of the diabatic barriers V_b^d. This is repeated for all values of the induced dipole moment d. A second approximation (adiabatic approximation) is to diagonalize this matrix (including the nondiagonal coupling terms) for each R and again find the maximum of the centrifugal barriers to get the height of the adiabatic barriers V_b^a. As an example, we compute these barrier heights for $^{40}\mathrm{K}\,{}^{87}\mathrm{Rb} - {}^{40}\mathrm{K}\,{}^{87}\mathrm{Rb}$ collisions, using a value of $C_6 = 16130$ a.u. [36]. We plot in Fig. 4 the heights of the diabatic (dashed lines) and adiabatic (solid lines) barriers for the quantum numbers $M_L = 0$ (red curves) and $|M_L| = 1$ (blue curves). The adiabatic barriers have been calculated using five partial waves $L = 1 - 9$ in Eq. (8). The effect of the couplings can be clearly seen in this figure by comparing diabatic and adiabatic barriers. Especially for the $|M_L| = 1$ case for $d \approx 0.16$ D (1 D = 1 Debye = 3.33610^{-30} Cm), couplings with higher partial waves make the adiabatic barrier decrease as the dipole increases while the diabatic barrier continues to increase.

Using these heights of the barriers, we use Eq. (11) to plot in Fig. 5 the total quenching rate coefficients (black curves)

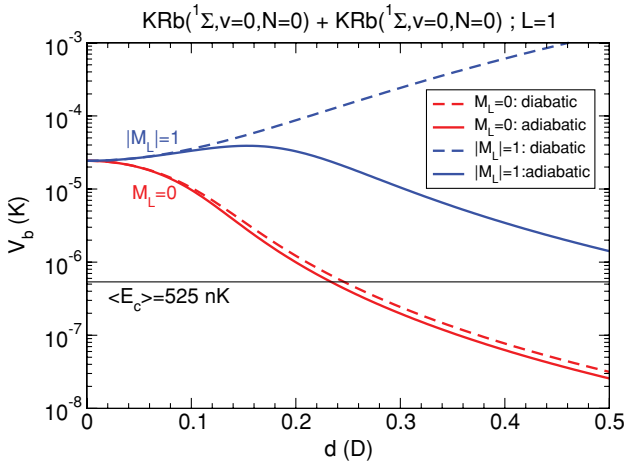

FIG. 4. (Color online) Diabatic (dashed lines) and adiabatic (solid lines) barrier heights $V_b^{d,a}$ as a function of the induced dipole moment d for the partial waves $L = 1$, $M_L = 0$ (red, lower) and $L = 1$, $|M_L| = 1$ (blue, upper).

as a function of d for two indistinguishable fermionic polar $^{40}K^{87}Rb$ molecules in the same quantum state for $L = 1$ and at a typical experimental temperature of $T = 350$ nK [32]. For $T = 350$ nK, the mean collision energy $\langle E_c \rangle = 3k_BT/2 = 525$ nK, and the maximum dipole moment for which $V_b < 525$ nK [that is for which Eq. (11) no longer applies] is around $d \approx 0.24$ D (see Fig. 4). The dashed curves correspond to rates calculated with the diabatic approximation while the solid curves correspond to rates calculated with the adiabatic approximation. The $M_L = 0$ contribution is plotted in red and the contribution of $M_L = +1$ and $M_L = -1$ is plotted in blue. The rates highly reflect the behavior of the centrifugal barriers in the entrance collision channel. When the barrier increases with the dipole, it prevents the molecules from getting close together and the quenching rates decreases. When the barrier decreases, the tunneling probability is increased allowing the molecules to get close together, and the quenching rates increase.

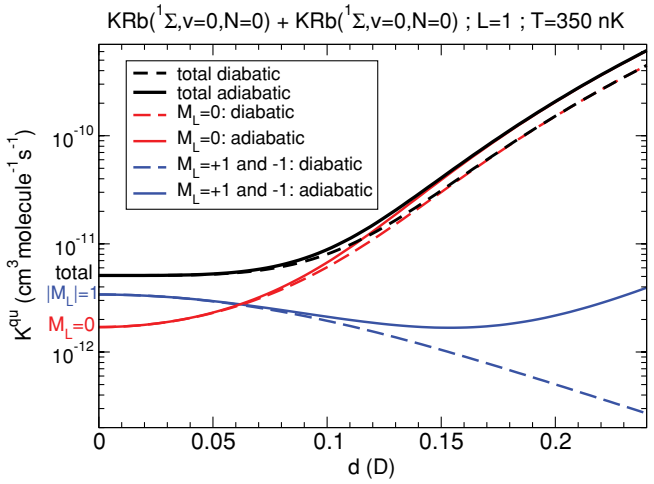

FIG. 5. (Color online) Quenching rate coefficients of two indistinguishable fermionic polar $^{40}K^{87}Rb$ molecules as a function of the induced electric dipole moment for $L = 1$ and for a temperature of $T = 350$ nK (black curves). The rates have been calculated using the barrier heights of Fig. 4. The red lines represent the $L = 1$, $M_L = 0$ partial-wave contribution. The blue lines represent the sum of $L = 1$, $M_L = 1$ and $L = 1$, $M_L = -1$ partial-wave contributions. The dashed lines represent the rates calculated with the diabatic barriers while the solid lines with the adiabatic barriers (see text for detail). The total, $M_L = 0$ and $|M_L| = 1$ curves have been indicated in the left-hand side.

2. *Analytical expressions*

In order to have an intuitive sense of how the chemical quenching rate scales with the induced dipole moment (and the electric field), we evaluate analytical expressions of the barriers and the rates as it has been done in the previous section for a zero electric field. The analytical expression of the height of the diabatic barrier V_b^d is complicated by the occurrence of two distinct long-range potentials in the diagonal matrix term of Eq. (8). We circumvent this difficulty by looking in the two limits where one dominates over the other. For small electric fields, we use the zero electric field limit discussed in the preceding section by setting $C_3 = 0$. For larger electric fields we ignore the C_6 coefficient in Eq. (8) if the electric dipole-dipole interaction is attractive (positive C_3). We ignore the centrifugal term in Eq. (8) if the electric dipole-dipole interaction is repulsive (negative C_3). These two cases are discussed below. In between, to accommodate the transition between the low-field and high-field limit, we will simply add the rate coefficients derived in the two limiting cases.

For positive C_3 coefficients in Eq. (9), $-C_3/R^3$ is attractive in Eq. (8). For $L = 1$ partial waves, for example, this occurs when $M_L = 0$, which favors an attractive orientation of dipoles. We consider

$$\left|\frac{C_3}{R^3}\right| \gg \left|\frac{C_6}{R^6}\right| \tag{15}$$

in Eq. (8). In this case, the position and height of the barrier are given by

$$\begin{aligned} R_b &= \frac{3\mu C_3}{\hbar^2 L(L+1)} \\ V_b &= \frac{[\hbar^2 L(L+1)]^3}{54\mu^3 C_3^2} \propto d^{-4}. \end{aligned} \tag{16}$$

The position of the barrier in Eq. (16) has to be in the region where Eq. (15) is satisfied. This happens for suitably large dipole moments, $d > d_a$ where

$$d_a = \left\{\frac{[\hbar^2 L(L+1)]^3 C_6 (4\pi\varepsilon_0)^4}{27\mu^3\alpha^4}\right\}^{1/8}. \tag{17}$$

The subscript a stands for the attractive interaction. For two indistinguishable fermionic polar $^{40}K^{87}Rb$ molecules, and for $L = 1$ and $M_L = 0$, $\alpha(1, 1; 0) = 4/5$ and we get $d_a = 0.103$ D. The threshold laws for quenching collisions in an electric field are the same as in the zero-field limit. Consequently, the quenching cross sections and rate coefficients behaves as in Eq. (11) except that V_b is given now by Eq. (16) and varies with d. We can insert Eq. (16) in Eq. (11) to get the corresponding analytical expressions. For a partial wave $L > 0$, the quenching rate scales as $d^{4(L+\frac{1}{2})}$. For two indistinguishable fermionic polar molecules at ultracold temperatures when $L = 1$ and

$M_L = 0$, we get

$$K^{qu}_{L=1,M_L=0} = \frac{3\pi}{8}\left(\frac{6^9\mu^6}{5^6\hbar^{14}}\right)^{1/2}\left(\frac{d^2}{4\pi\varepsilon_0}\right)^3 k_B T\Delta. \quad (18)$$

Thus the $L = 1$, $M_L = 0$ quenching rate increases as d^6. This is a more rapid dependence on dipole moment than for purely long-range dipolar relaxation in dipolar gases [4].

For negative C_3 coefficients in Eq. (9), $-C_3/R^3$ is repulsive in Eq. (8). For $L = 1$ partial waves, for example, this occurs when $M_L = \pm 1$, which favors a repulsive orientation of dipoles. We consider

$$\left|\frac{C_3}{R^3}\right| \gg \left|\frac{\hbar^2 L(L+1)}{2\mu R^2}\right| \quad (19)$$

in Eq. (8). The long-range potential again experiences a barrier, but now it is generated by the balance between the repulsive dipole potential at large R, and the attractive van der Waals potential at somewhat smaller R. In this case, the position and height of this barrier are given by

$$R_b = \left(\frac{2C_6}{|C_3|}\right)^{1/3}$$
$$V_b = \frac{|C_3|^2}{4C_6} \propto d^4. \quad (20)$$

For this approximation to hold, the position of the barrier in Eq. (20) has to be in the region where Eq. (19) is satisfied. This requires that $d > d_r$ where

$$d_r = \left\{\frac{[\hbar^2 L(L+1)]^3 C_6 (4\pi\varepsilon_0)^4}{4\mu^3\alpha^4}\right\}^{1/8}. \quad (21)$$

The subscript r stands for the repulsive interaction. For two indistinguishable fermionic polar ^{40}K^{87}Rb molecules, and for $L = 1$ and $M_L = 1$ or $M_L = -1$, $\alpha(1, 1; \pm 1) = 2/5$ and we get $d_r = 0.186$ D. We can replace Eq. (20) in Eq. (11) to get the corresponding analytical expressions. For a partial wave $L > 0$, the quenching processes scale as $d^{-4(L+\frac{1}{2})}$. For two indistinguishable fermionic polar molecules at ultracold temperatures when $L = 1$ and $|M_L| = 1$, we get

$$K^{qu}_{L=1,|M_L|=1} = \frac{3\pi}{8}\left(\frac{50\hbar^{\frac{4}{3}}C_6}{\mu}\right)^{3/2}\left(\frac{d^2}{4\pi\varepsilon_0}\right)^{-3} k_B T\Delta. \quad (22)$$

The $L = 1$, $|M_L| = 1$ quenching rate decreases as d^{-6} as the electric field grows.

These analytical expressions use the diabatic barriers. If we consider that at large d, the total rate is mostly given by the $M_L = 0$ contribution (we neglect the $|M_L| = 1$ contributions at large d), one can have an analytical expression using the adiabatic barrier. If we take into account the couplings between $L = 1, M_L = 0$ and $L = 3, M_L = 0$, we can diagonalize analytically the 2×2 matrix in Eq. (8). It can be shown that for each dipole moment d, the coupling with $L = 3, M_L = 0$ lower the diabatic barrier of $L = 1, M_L = 0$ by a factor of 0.76 at the position of the barrier, to give rise to the adiabatic barrier. Inserting this correction of the barrier in Eq. (11), this yields a correction of $0.76^{-3/2} \approx 1.51$ for $K^{qu}_{L=1,M_L=0}$. The difference between diabatic and adiabatic calculations can be already seen in Fig. 4 and Fig. 5 for the numerical barriers at large dipole moment.

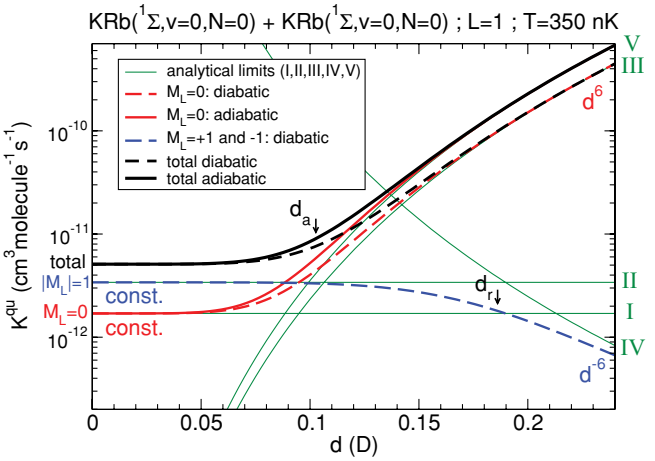

FIG. 6. (Color online) Same as Fig. 5 but we use the analytical expressions for the rates (see text for detail). The total, $M_L = 0$ and $|M_L| = 1$ curves have been indicated in the left-hand side. The individual analytical curves have been indicated in the right-hand side by roman numbers.

In Fig. 6 the black curve corresponds to the total quenching rate coefficient as a function of d for two indistinguishable fermionic polar ^{40}K^{87}Rb molecules in the same quantum state for $L = 1$ and at a temperature of $T = 350$ nK. The analytical expressions I, II, III, IV, V (green thin lines) correspond respectively to Eq. (13), 2 × Eq. (13), Eq. (18), 2 × Eq. (22), 1.51× Eq. (18). The curves III and IV are for the diabatic barriers, while curve V is to account for the adiabatic barrier. The red dashed line (I+III) represents the $L = 1, M_L = 0$ partial-wave contribution for the diabatic barriers while the blue dashed line (II+IV) represents the sum of $L = 1, M_L = 1$ and $L = 1, M_L = -1$ partial-wave contributions for the diabatic barriers. The analytical sum I+II+III+IV is represented as a black dashed line. To account for the adiabatic barriers we assume that the correction for the total rate comes only from the $L = 1, M_L = 0$ partial wave, and we replace I+III by I+V (red solid line). The analytical sum I+II+V+IV is represented as a black solid line. Neglecting the d^{-6} contribution at larger d, the analytical p-wave quenching rate (taking into account the adiabatic barriers) is given by the simple expression

$$K^{qu}_{L=1} = \frac{\pi}{8}\left\{p_1\left(\frac{3^{17}\mu^3 C_6^3}{\hbar^{10}}\right)^{1/4} + 1.51 p_2\left(\frac{2^9 3^{11}\mu^6}{5^6\hbar^{14}}\right)^{1/2} \times \frac{d^6}{(4\pi\varepsilon_0)^3}\right\} k_B T\Delta. \quad (23)$$

p_1 (p_2) is the quenching probability reached at the height of the barrier in the QT model for the zero (nonzero) electric field regime. The QT model assumes that $p_1 = p_2 = 1$ but become fitting parameters (p_1, $p_2 < 1$) when compared with full quantum calculations or experimental data. The limiting value $d_a = 0.103$ D ($d_r = 0.186$ D), where the

d^6 (d^{-6}) behavior begins, has also been indicated with an arrow. It turns out that the total rates for $L = 1$ calculated analytically (for both the use of diabatic and adiabatic barriers) are very similar to the numerical ones of Fig. 5 (10% difference at most, around d_a). However, the subcomponents $L = 1, M_L = 0$ and $L = 1, |M_L| = 1$ have different behaviors. For example the numerical $L = 1, M_L = 0$ ($L = 1, |M_L| = 1$) component starts to increase (decrease) at earlier dipole moment (typically at 0.02 D) than their analytical analogs (typically after 0.06 D). The use of the simple analytical expressions (using the diabatic or adiabatic barriers) can be useful to estimate the total rate coefficients, while the numerical ones are prefered to estimate the $L = 1, M_L = 0$ and $L = 1, |M_L| = 1$ individual rates.

III. PROSPECTS FOR COLLISIONS IN TWO DIMENSIONS

In three-dimensional collisions, the quenching loss is largely due to incident partial waves with angular-momentum projection $M_L = 0$, emphasizing head-to-tail orientations of pairs of dipoles. These are the kind of collisions that are largely suppressed in traps with a pancake geometry, with the dipole polarization axis orthogonal to the plane of the pancake [37]. If these collisions can be removed, then it is likely that increasing the electric field will suppress quenching collisions, making evaporative cooling possible. If we assume an ideal pancake trap that confines the particles to move strictly on a plane, one can apply the present model to estimate the behavior of the quenching processes. We assume that the molecules are polarized along the electric field axis, perpendicular to the two-dimensional plane. In this case, the long-range potential is given by

$$V(\rho) = \frac{\hbar^2(|M|^2 - 1/4)}{2\mu\rho^2} - \frac{C_6}{\rho^6} + \frac{d^2}{4\pi\varepsilon_0\rho^3}, \tag{24}$$

where ρ stands for the distance between two particles in a two-dimensional plane and M stands for the angular-momentum projection on the electric field axis. The last term comes from the repulsive dipole-dipole interaction when the dipoles are pointing along the electric field and approach each other side by side. The height of this barrier has been plotted as a function of d in Fig. 7 (black solid line). At ultralow energy and large molecular separation, the Bethe-Wigner laws for quenching processes depend only on the long-range repulsive centrifugal term $1/R^2$ [31,38]. The repulsive centrifugal terms are different in Eq. (8) and Eq. (24). As the repulsive centrifugal term in Eq. (8) leads to the threshold laws in Eq. (10), the replacement $L(L+1) \to |M|^2 - 1/4$ (that is $L \to |M| - 1/2$) in Eq. (10) leads to

$$\left|T_M^{qu}\right|^2 = \left(\frac{E_c}{V_b}\right)^{|M|}, \tag{25}$$

where V_b denotes the height of the centrifugal barrier in two dimensions. This result requires that the centrifugal potential is repulsive, i.e., that $|M| > 0$. For $M = 0$ the threshold law exhibits instead a logarithmic divergence [31].

In two dimensions, quenching cross sections and rate coefficients have, respectively, units of length and length

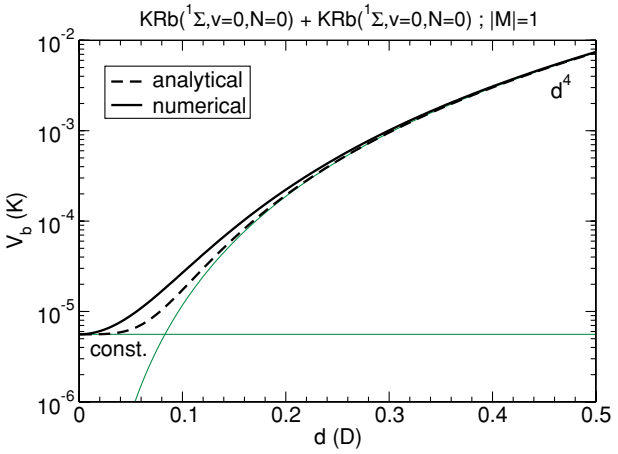

FIG. 7. (Color online) Barrier heights as a function of the induced dipole moment d for the partial waves $|M| = 1$ in two dimensions. The green thin curves represent the analytical Eq. (28) (constant) and Eq. (29) (d^4). The dashed black curve is the sum of them. The solid black curve is the height of the barrier in Eq. (24).

squared per unit of time and are given by [39]

$$\begin{aligned} \sigma_M^{qu} &= \frac{\hbar}{\sqrt{2\mu E_c}}\left|T_M^{qu}\right|^2\Delta \\ K_M^{qu} &= \frac{\hbar}{\mu}\left|T_M^{qu}\right|^2\Delta. \end{aligned} \tag{26}$$

Within this model, it follows that the quenching cross section and rate coefficient for $|M| > 0$ are given by

$$\begin{aligned} \sigma_M^{qu} &= \frac{\hbar}{\sqrt{2\mu}V_b^{|M|}}\, E_c^{|M|-1/2}\Delta \\ K_M^{qu} &= \frac{\hbar}{\mu V_b^{|M|}}\,\langle E_c^{|M|}\rangle\Delta. \end{aligned} \tag{27}$$

The energy dependence is in agreement with the one found in Ref. [40]. In Eq. (27),

$$V_b = \left\{\frac{[\hbar^2(|M|^2 - 1/4)]^3}{54\mu^3 C_6}\right\}^{1/2} \tag{28}$$

for the zero-electric field regime and

$$V_b = \frac{1}{4C_6}\left(\frac{d^2}{4\pi\varepsilon_0}\right)^2 \tag{29}$$

for the nonzero electric field regime. The height of these barriers has been reported in Fig. 7 (green thin lines). These results imply that for $|M| = 1$ the quenching processes within this model will be independent of the dipole moment in the zero electric field regime, where

$$K_{|M|=1}^{qu} = \left(\frac{2^7\mu C_6}{\hbar^4}\right)^{1/2} k_B T\Delta \tag{30}$$

and will scale as d^{-4} in the nonzero electric field regime, where

$$K_{|M|=1}^{qu} = \frac{4\hbar C_6}{\mu}\left(\frac{d^2}{4\pi\varepsilon_0}\right)^{-2} k_B T\Delta. \tag{31}$$

We use the fact that $\langle E_c\rangle = k_B T$ in two dimensions. The nonzero electric field regime is reached when $d > d_{2D}$

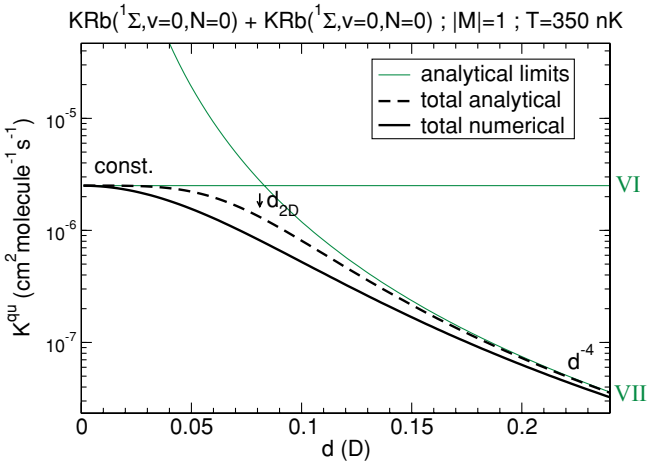

FIG. 8. (Color online) Two dimensional quenching rate coefficient (black curves) of two indistinguishable fermionic polar $^{40}K^{87}Rb$ molecules as a function of the induced electric dipole moment for the $M = 1$ and $M = -1$ components at a temperature of $T = 350$ nK. The dashed lines represent the rate using analytical expressions while the solid line represents the rate using the numerical expression (see text for detail). The individual analytical curves have been indicated in the right-hand side by roman numbers.

where

$$d_{2D} = \left\{ \frac{[\hbar^2(|M|^2 - 1/4)]^3 C_6 (4\pi\varepsilon_0)^4}{4\mu^3} \right\}^{1/8}. \qquad (32)$$

For two indistinguishable fermionic polar $^{40}K^{87}Rb$ molecules, and for $|M| = 1$, we get $d_{2D} = 0.081$ D.

The behavior of the quenching rate (black lines) is shown in Fig. 8 for two indistinguishable fermionic polar $^{40}K^{87}Rb$ molecules as a function of the induced electric dipole moment for $M = 1$ and $M = -1$ components at a temperature of $T = 350$ nK. The dashed line represents the analytical rate which is the sum of the analytical expression VI corresponding to $2 \times$ Eq. (30) and analytical expression VII corresponding to $2 \times$ Eq. (31). The solid line represents the rate using the general expression Eq. (27) and the numerical height of the barrier calculated in Eq. (24). The limiting value $d_{2D} = 0.081$ D, where the d^{-4} behavior for the quenching rate begins, has also been indicated with an arrow. The difference between the numerical calculation and the analytical expression reflects the difference in the calculation of the height of the barrier, already seen in Fig. 7. The numerical calculation is more exact, while the other is analytical. However, at large d, the numerical rate tends to the analytical d^{-4} behavior. The quenching rate decreases rapidly as the dipole moment increases and this may be promising for efficient evaporative cooling of polar molecules since the elastic rate is expected to grow with increasing dipole moment [41].

IV. CONCLUSION

We have proposed a simple model which combines quantum threshold laws and a classical capture model to determine analytical expressions of the chemical quenching cross section and rate coefficient as a function of the collision energy or the temperature. We also provide an estimate as a function of the induced electric dipole moment d in the presence of an electric field. We found that the quenching rates of two ultracold indistinguishable fermionic polar molecules grows as the sixth power of d. For weaker electric field, quenching processes are independent of the induced electric dipole moment. Prospects for two-dimensional collisions have been discussed using this model and we predict that the quenching rate will decrease as the inverse of the fourth power of d. This fact may be useful for efficient evaporative cooling of polar molecules. This model provides a general and comprehensive picture of ultracold collisions in electric fields. Preliminary data suggest that this model gives good agreement with experimental chemical rates for three-dimensional collisions in an electric field [42].

ACKNOWLEDGMENTS

We acknowledge the financial support of NIST, the NSF, and an AFOSR MURI grant. We thank K.-K. Ni, S. Ospelkaus, D. Wang, M. H. G. de Miranda, B. Neyenhuis, P. S. Julienne, J. Ye, and D. S. Jin for helpful discussions.

[1] J. M. Sage, S. Sainis, T. Bergeman, and D. DeMille, Phys. Rev. Lett. **94**, 203001 (2005).
[2] K.-K. Ni, S. Ospelkaus, M. H. G. de Miranda, A. Pe'er, B. Neyenhuis, J. J. Zirbel, S. Kotochigova, P. S. Julienne, D. S. Jin, and J. Ye, Science **322**, 231 (2008).
[3] J. Deiglmayr, A. Grochola, M. Repp, K. Mörtlbauer, C. Glück, J. Lange, O. Dulieu, R. Wester, and M. Weidemüller, Phys. Rev. Lett. **101**, 133004 (2008).
[4] S. Hensler *et al.*, Appl. Phys. B **77**, 765 (2003).
[5] J. L. Bohn, M. Cavagnero, and C. Ticknor, New J. Phys. **11**, 055039 (2009).
[6] A. V. Avdeenkov and J. L. Bohn, Phys. Rev. A **66**, 052718 (2002).
[7] N. Balakrishnan and A. Dalgarno, Chem. Phys. Lett. **341**, 652 (2001).
[8] P. Soldán, M. T. Cvitaš, J. M. Hutson, P. Honvault, and J.-M. Launay, Phys. Rev. Lett. **89**, 153201 (2002).
[9] G. Quéméner, P. Honvault, and J.-M. Launay, Eur. Phys. J. D **30**, 201 (2004).
[10] G. Quéméner, P. Honvault, J.-M. Launay, P. Soldán, D. E. Potter, and J. M. Hutson, Phys. Rev. A **71**, 032722 (2005).
[11] M. T. Cvitaš, P. Soldán, J. M. Hutson, P. Honvault, and J.-M. Launay, Phys. Rev. Lett. **94**, 033201 (2005).
[12] M. T. Cvitaš, P. Soldán, J. M. Hutson, P. Honvault, and J.-M. Launay, Phys. Rev. Lett. **94**, 200402 (2005).
[13] M. Lara, J. L. Bohn, D. Potter, P. Soldán and J. M. Hutson, Phys. Rev. Lett. **97**, 183201 (2006).
[14] G. Quéméner, J.-M. Launay, and P. Honvault, Phys. Rev. A **75**, 050701(R) (2007).
[15] J. M. Hutson and P. Soldán, Int. Rev. Phys. Chem. **26**, 1 (2007).

[16] G. Quéméner, N. Balakrishnan, and A. Dalgarno, in *Cold Molecules: Theory, Experiment, Applications*, edited by R. V. Krems, W. C. Stwalley, and B. Friedrich (CRC Press, Boca Raton, FL, 2009).
[17] G. Quéméner, N. Balakrishnan, and B. K. Kendrick, Phys. Rev. A **79**, 022703 (2009).
[18] P. Langevin, Ann. Chim. Phys. **5**, 245 (1905).
[19] P. Julienne and F. H. Mies, J. Opt. Soc. Am. B **6**, 2257 (1989).
[20] J. P. Burke Jr., C. H. Greene, and J. L. Bohn, Phys. Rev. Lett. **81**, 3355 (1998).
[21] F. H. Mies and M. Raoult, Phys. Rev. A **62**, 012708 (2000).
[22] P. S. Julienne, Faraday Discuss. **142**, 361 (2009).
[23] C. Orzel, M. Walhout, U. Sterr, P. S. Julienne, and S. L. Rolston, Phys. Rev. A **59**, 1926 (1999).
[24] E. R. Hudson, N. B. Gilfoy, S. Kotochigova, J. M. Sage, and D. DeMille, Phys. Rev. Lett. **100**, 203201 (2008).
[25] E. R. Hudson, C. Ticknor, B. C. Sawyer, C. A. Taatjes, H. J. Lewandowski, J. R. Bochinski, J. L. Bohn, and J. Ye, Phys. Rev. A **73**, 063404 (2006).
[26] T. V. Tscherbul and R. V. Krems, J. Chem. Phys. **129**, 034112 (2008).
[27] J. P. Burke Jr., Ph.D. thesis, University of Colorado (1999), available online at http://jilawww.colorado.edu/pubs/thesis/burke.
[28] S. Ospelkaus, K.-K. Ni, G. Quéméner, B. Neyenhuis, D. Wang, M. H. G. de Miranda, J. L. Bohn, J. Ye, and D. S. Jin, Phys. Rev. Lett. **104**, 030402 (2010).
[29] H. A. Bethe, Phys. Rev. **47**, 747 (1935).
[30] E. P. Wigner, Phys. Rev. **73**, 1002 (1948).
[31] H. R. Sadeghpour *et al.*, J. Phys. B: At. Mol. Opt. Phys. **33**, R93 (2000).
[32] S. Ospelkaus, K.-K. Ni, D. Wang, M. H. G. de Miranda, B. Neyenhuis, G. Quéméner, P. S. Julienne, J. L. Bohn, D. S. Jin, and J. Ye, e-print arXiv:0912.3854, Science, in press (2010).
[33] Z. Idziaszek and P. S. Julienne, e-print arXiv:0912.0370, submitted (2009).
[34] J. Aldegunde, B. A. Rivington, P. S. Zuchowski, and J. M. Hutson, Phys. Rev. A **78**, 033434 (2008).
[35] J.-M. Launay and M. Le Dourneuf, Chem. Phys. Lett. **163**, 178 (1989).
[36] S. Kotochigova (private communication, 2009).
[37] A. Micheli, G. Pupillo, H. P. Büchler, and P. Zoller, Phys. Rev. A **76**, 043604 (2007).
[38] A. R. P. Rau, Comments At. Mol. Phys. **14**, 285 (1984).
[39] P. Naidon and P. S. Julienne, Phys. Rev. A **74**, 062713 (2006).
[40] Z. Li, S. V. Alyabyshev, and R. V. Krems, Phys. Rev. Lett. **100**, 073202 (2008).
[41] C. Ticknor, Phys. Rev. A **80**, 052702 (2009).
[42] K.-K. Ni, S. Ospelkaus, D. Wang, G. Quéméner, B. Neyenhuis, M. H. G. de Miranda, J. L. Bohn, J. Ye, and D. S. Jin, e-print arXiv:1001.2809, submitted (2010).